Appendix A. Electronic Supplementary Information

Anaerobic dissolved As(III) removal from metal-polluted waters by cathode-stabilized Fe(III)-oxyhydroxides

Astolfo Valero[1,2], **Jiří Jan**[1], **Daniel A. Petrash**[1,3]

[1]*Biology Centre of the Czech Academy of Sciences, Institute of Soil Biology and Biogeochemistry, Na Sádkách 7, 370 05 České Budějovice, Czech Republic*

[2] *University of South Bohemia, Department of Ecosystem Biology, Branisovská 1645/31a, 370 05 České Budějovice, Czech Republic*

[3]*Department of Environmental Geochemistry and Biogeochemistry, Czech Geological Survey, 152 00 Prague 5, Czech Republic*

Electronic Supplementary Information 1 (S1): Methods details

S1.1 Microorganism's culturing

A pure strain of *Geobacter* sp. (DSM 11489), capable of extracellular electron transfer to insoluble materials, was selected as a model electroactive bacterium for our bioelectrochemical systems (BES). This strain was obtained in its exponential growth phase from the German Collection of Microorganisms and Cell Cultures (Leibniz Institute, Germany). Bacterial suspensions (10% v/v) were enriched in glass sterile Hungate-type tubes that held anaerobes growth medium (90% v/v, DSM 503) containing 20 mM of acetate and 40 mM of fumarate as electron donor and terminal electron acceptor, respectively (after ref. 1). These were incubated anaerobically at 30 °C (Coy, USA) until cultures reached values of 1 in the McFarland Standards scale (DEN-1 McFarland Densitometer; Biosan, Latvia), which corresponds to ca. $3x10^{-8}$ $CFUmL^{-1}$ (as described by ref. 2). Afterwards, bacteria's cells were harvested and transferred to electrochemical reactions vessels (100 mL) before starting chronoamperometric assays. All procedures were performed inside an anaerobic chamber (Coy, USA) under N_2 atmosphere (O_2 < 1.5 µg L^{-1}).

S1.2 Calculation of arsenic's partition coefficient (Kd)

We amended our BES with environmentally relevant concentrations of As that were consistent with observed distribution coefficients between the ferruginous water and sediments (Fig. S3). The partition coefficient (Kd) was calculated as described in ref. 3, and following equation 1:

$$K_d = \frac{\left(As\ concentration \,/\, Al\ concentration\right)_{sediment}}{\left(As\ concentration \,/\, Al\ concentration\right)_{water}}$$

Eq. 1

As concentrations were normalized by using Al (i.e., conservative element) to ensure that Kd values reflected the natural geochemical background of our model site. Kd values were calculated for the ferruginous anoxic monimolimnion (50–55 m) and sediments (4 cm depth) of Lake Medard. These indicate that As content in the sediment-water interface (SWI) could be *ca.* 23x higher than those found near the lake's redoxcline, and that As is likely exported to the water column from the sediment.

S1.3 Characterization of humic substance derivatives extracted from leonardite standard

Fluorescence spectroscopy was used to obtain an exploratory characterization of the humic acid amendment employed, *i.e.* leonardite standard (IHSS, USA). Excitation-emission matrices were measured using a Duetta Spectrophotometer (Horiba, Japan) with excitation wavelengths in the range of 250 to 550 nm (5 nm increment steps) and emission wavelengths in the range of 250–800 nm (1 nm increment step). The fluorescence values obtained were compared with those of (a) dissolve organic matter from Lake Medard; and with (b) organic matter extracted from commercial humic acids (Sigma Aldrich). Fluorescence peaks are shown in Table S1 and indicate that the leonardite amendment contained analogous humic acid derivatives to those found in commercially

available humic acids. These values also indicate that aromatic derivatives domain the dissolved organic matter from the anoxic water of our model site. These results validated the utilization of leonardite derivatives as a source of humic acids for our BES.

S1.4 Synchrotron-based X-ray analyses

Spatially resolved synchrotron-based X-ray fluorescence (μ-XRF), angle-resolved diffraction (μ-XRD), and absorption (μ-XAS) were performed by turning the instrument at ca. 11.95 keV and by focusing the beam with a Kirkpatrick–Baez (KB) mirror system. Simultaneous μ-XRF and μXRD scanning was conducted in the same polarization plane at 1x1 μm^2 (HxV) resolution. The energy of the X-ray beam was tuned using a fixed-exit monochromator equipped with a pair of Si (111) crystals. For μ-XRF was used a silicon drift detector (Ketek) mounted at 90° angle to the incident beam; whereas for μ-XRD was utilized a hybrid photon counting detector. A dwelling-time of 200 ms per scanned point was applied to acquire μ-XRF maps. Such resolution was sufficient to identify relevant Fe-As hotspots (i.e., on precipitated aggregates) on the surfaces of sliced working electrodes and filtrates. The diffraction pattern of a standard polycrystalline sample of La_2B_3 was used to calibrate an EIGER 4M detector position with respect to the sample. The measured 2D diffraction patterns images in the sampled regions resulted in powder rings data, which were then azimuthally integrated by using the software XRDUA[4]. Match! Software[1] (version 3.12) was used for the identification of mineral phases by comparison of the resulting XRD patterns with the Crystallography Open Database (COD) and RRUFF mineral databases[5] (Fig. S8). X-ray absorption spectra through the As K-edge were measured throughout X-ray absorption near-edge structure (XANES) spectroscopy to detect As coordination and redox state. The spectra were acquired by scanning the primary energy around the As K-edge at 11.8 to 12.6 keV with a step of 0.5 eV. In each interest point, 5 to 6 scans were performed depending on data quality. Resulting spectra were fit with linear combinations of component spectra using a non-linear least-squares algorithm employing Athena's open-source code which implements IFEFFIT[6].

[1] Match! - Phase Analysis using Powder Diffraction, Crystal Impact - Dr. H. Putz & Dr. K. Brandenburg GbR, Kreuzherrenstr. 102, 53227 Bonn, Germany, https://www.crystalimpact.de/match.

Table S1. Characterization of the humic-like and protein peaks, and relative proportion of aromatics compounds comprising the humic substances derivatives extracted from Lake Medard's anoxic monimolimnion, commercially-available humic acids and the IHS leonardite standard.

	Humic-like peaks			Protein peaks		Aromatic's proportion
	A	m	C	B	T	(%)
Lake Medard anoxic water	2.9	0.6	0.4	0.0	1.4	73
Commercial humic acid	69.7	19.2	10.7	11.0	10.9	82
Leonardite standard	61.2	19.6	10.4	2.1	6.3	92

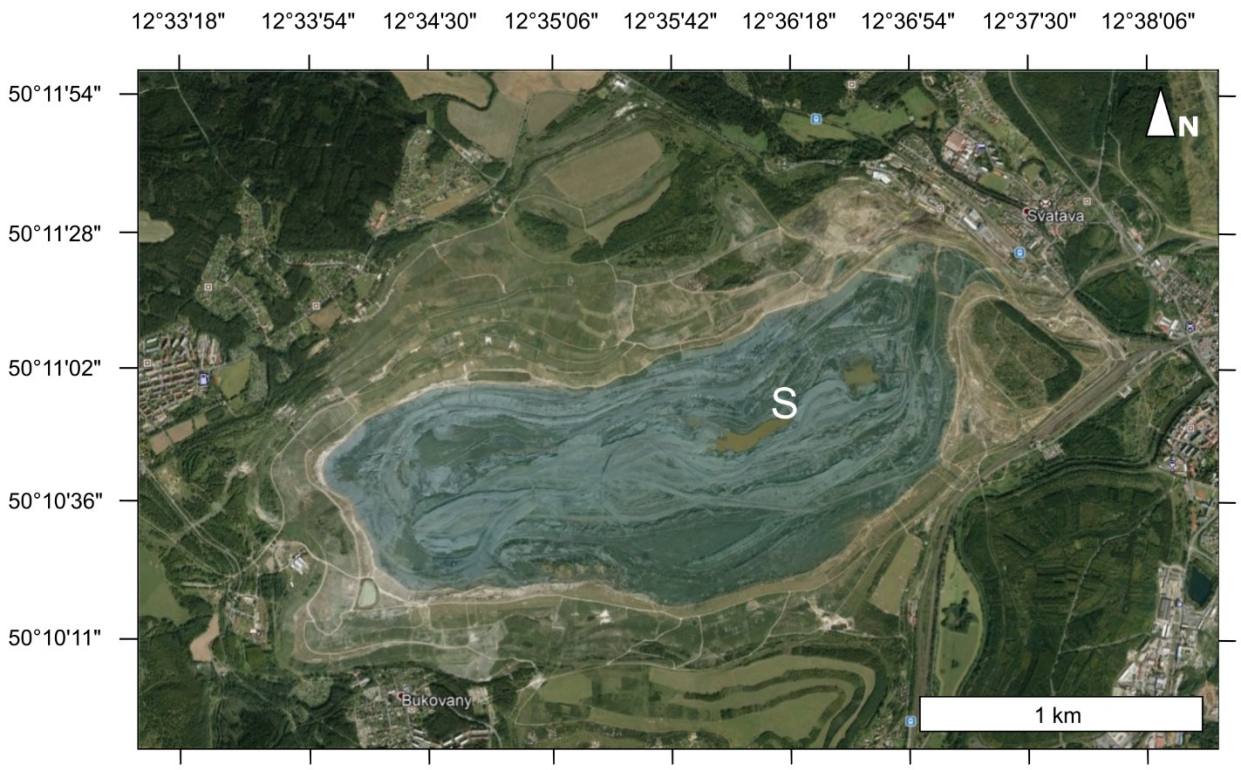

Figure S1. Post-mining lake Medard (Karlovy Vary region, NW Czech Republic; blue area) formed after flooding of the Medard-Libík lignite mine (background). Brown areas indicate past pit lakes, and are the current deepest and permanently redox stratified depressions of the artificial lake bed. "S" indicates the sampling location of water samples. Satellite imagery was extracted from Google Earth® in June 2021.

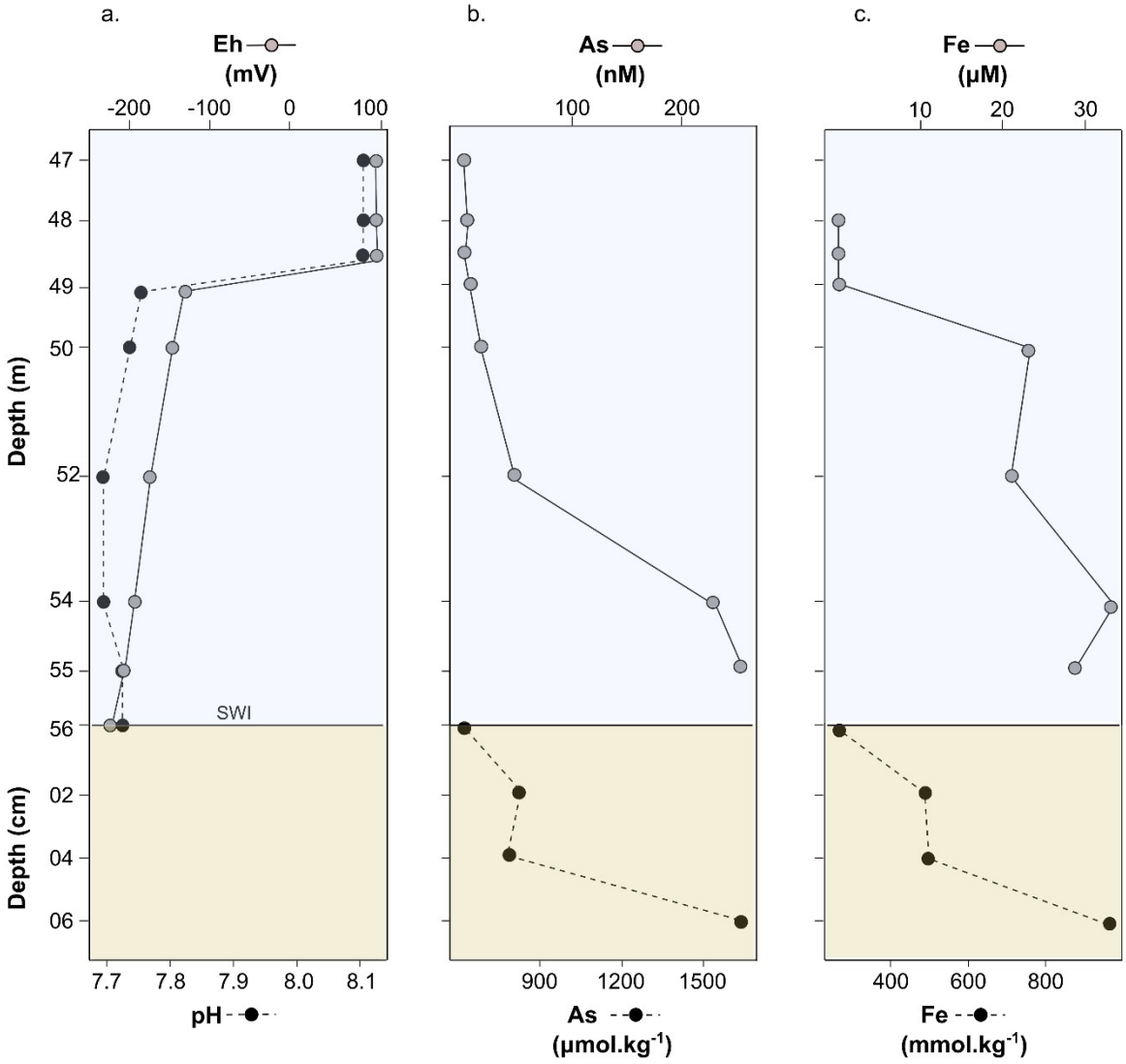

Figure S2. Depth-dependant profiles of physic-chemical parameters (a): redox potential (grey) and pH (black) in the water column (light blue), and redox-reactive metal(loid)s concentration of arsenic (b) and iron (c) in the anoxic monimolimnion (light blue) and the sediments (light brown) of the post-mining lake Medard (November 2019). Black horizontal line placed at 56 m depth indicates the sediment-water interface (SWI).

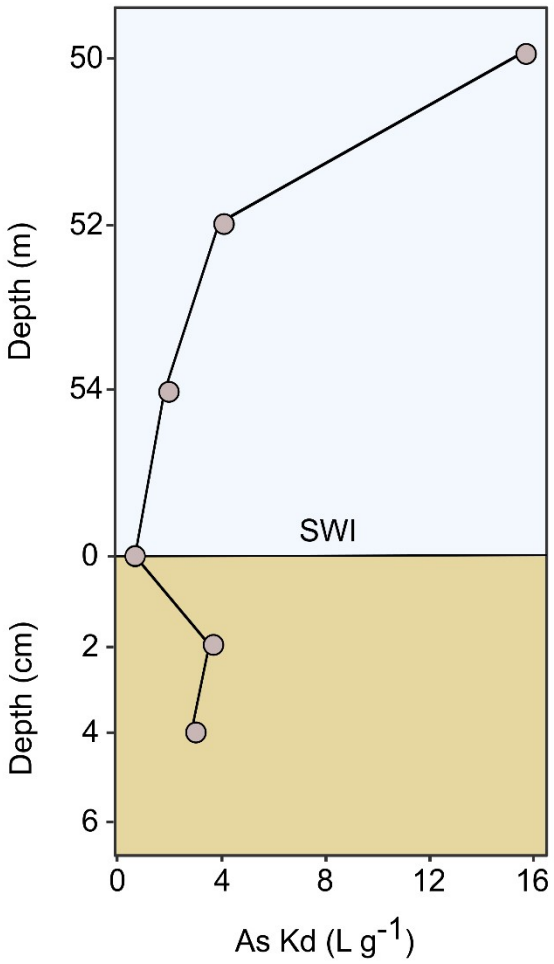

Fig. S3. Partition coefficient (Kd) of As in both the ferruginous anoxic monimolimnion (50-55 m, light blue) and sediments (4 cm depth, light brown) of Lake Medard. The sediment calculation extrapolates the dissolved As concentration measured at the sediment-water interface (SWI, *i.e.,* black horizontal line placed at 55 m depth).

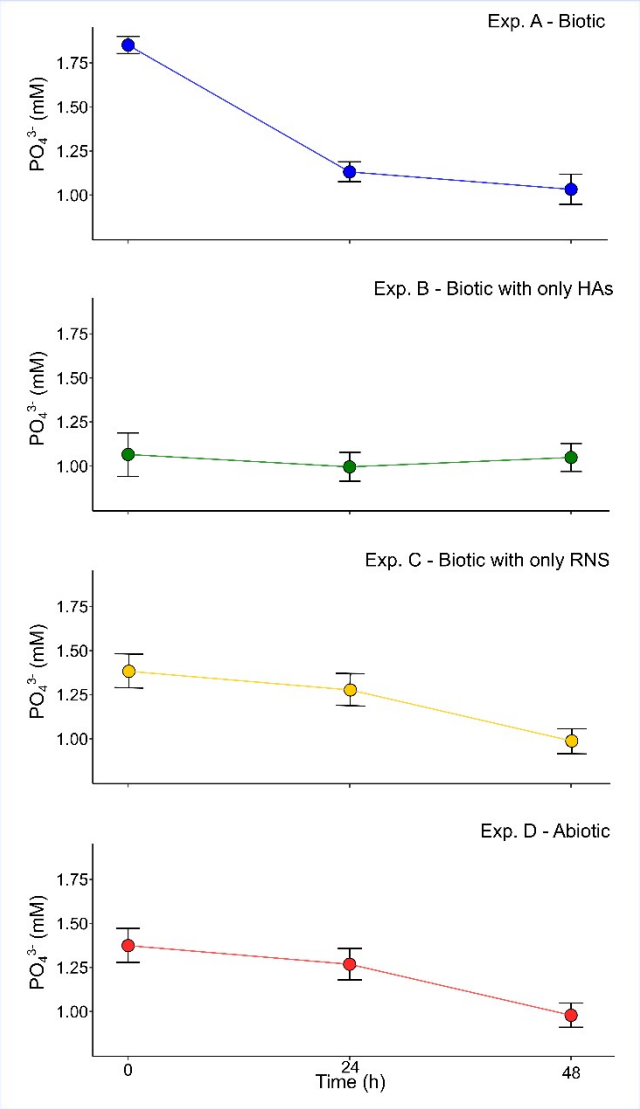

Figure S4. Phosphate (PO_4^{3-}) content determined at sampling times t = 0, 24, and 48 h as the following chronoamperometric assays proceeded: (1) synthetic ferruginous solutions amended with both reactive nitrogen species (RNS) and humic acid derivatives (HAs; Exp. A); (2) synthetic ferruginous solutions with HAs, but lacking RNS (Exp. B); (3) synthetic ferruginous solutions with RNS and no HAs added (Exp. C); and (4) an abiotic control of Exp. A (Exp. D). Experimental/analytical standard errors are shown.

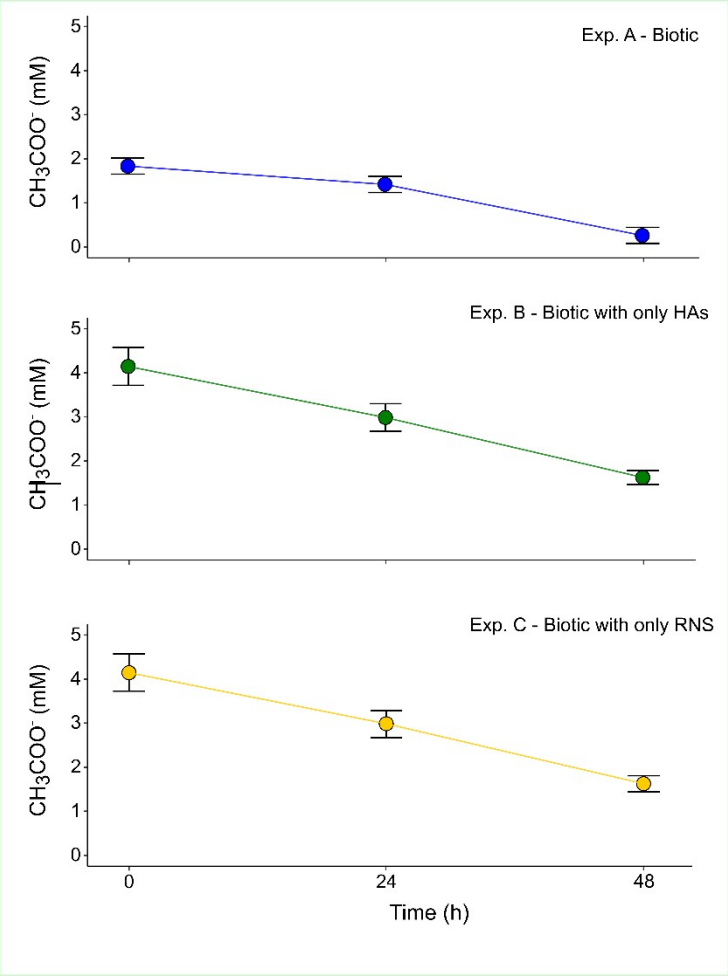

Figure S5. Acetate (CH_3COO^-) ion contents measured at t = 0, 24, and 48 h as the following biotic chronoamperometric assays progressed: (1) synthetic ferruginous solutions amended with both RNS and HAs (Exp. A); (2) synthetic ferruginous solutions with HAs, but lacking RNS (Exp. B); and (3) synthetic ferruginous solutions with RNS and no HAs added (Exp. C).

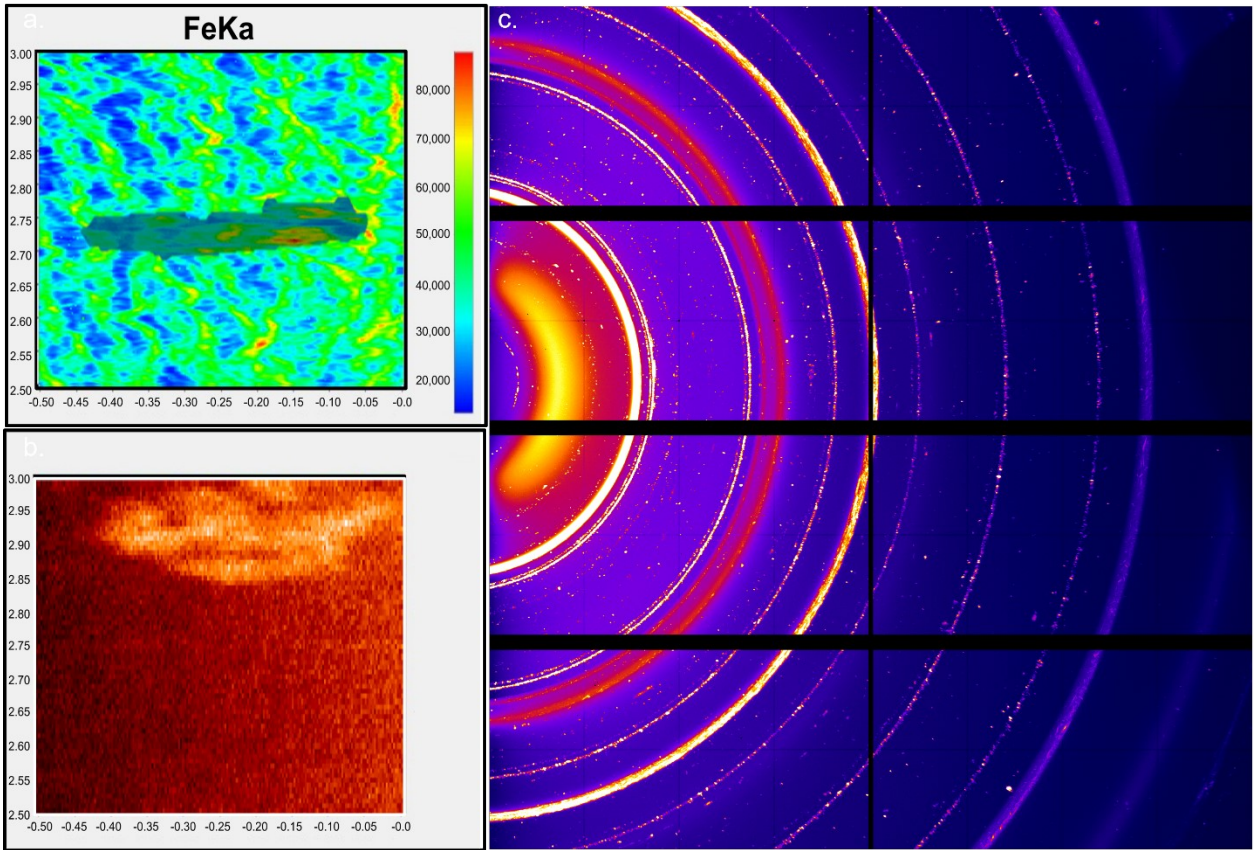

Figure S6. Illustrative figure displaying (a) an individual μ-XRF map showing a non-uniform elemental distribution of Fe (colored background) and As (shadowed area) on electrode surfaces from biotic chronoamperometric assays; and (b) the presence of crystalline mineral phases, on these As-Fe elemental hotspots, from which we obtained (c) individual 2D XRD patterns.

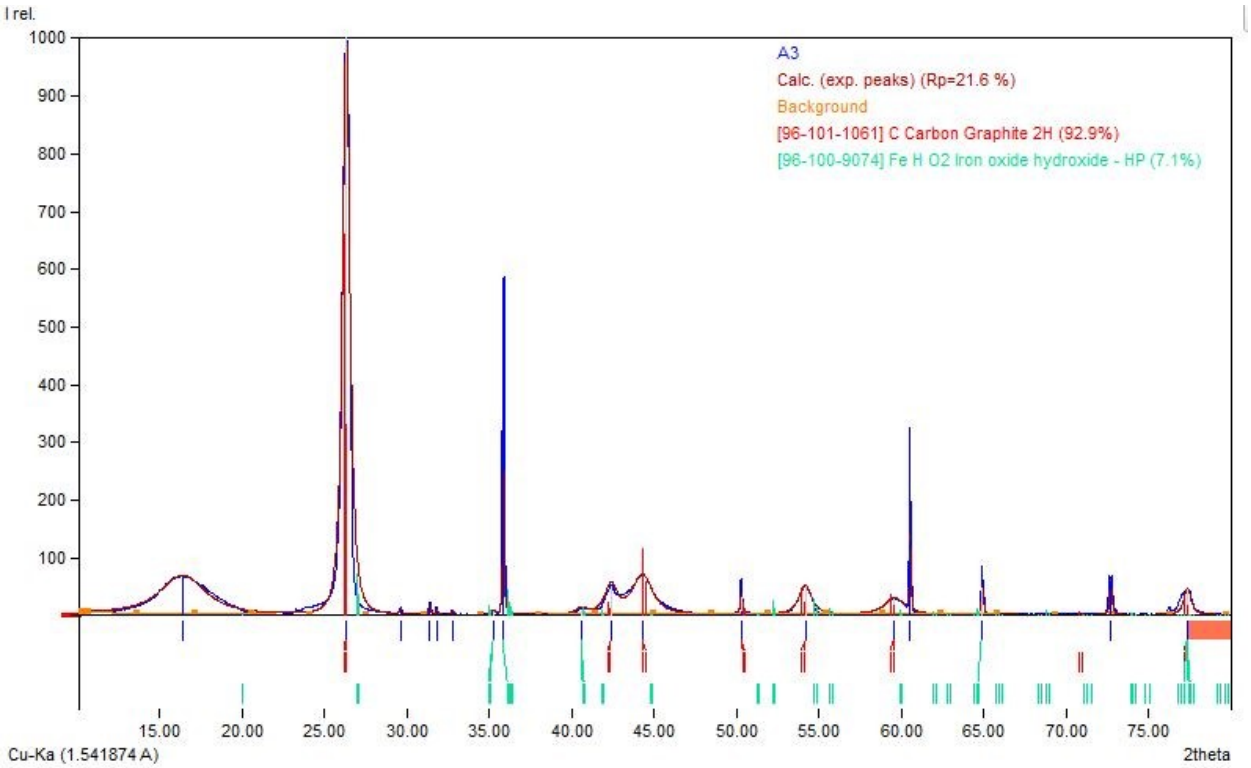

Figure S7. Representative synchrotron-based μ-XRD diffraction pattern indicating the occurrence of poorly crystalline Fe(III) oxyhydroxide mineral phases (*ca.* 7 wt%) on graphite cathode surfaces. The sample was collected after 48 h, and it is representative of those synthesized in biotic chronoamperometric assays biotic amended with RNS but no humic acid derivative addition. For comparison purposes—*i.e.,* to evaluate peak matches using database-listed phases (see S1.4 above)—the 1D patterns from diffractions collected at the beamline (11.95 keV) were transformed to Cu-Ka1-equivalent patterns.

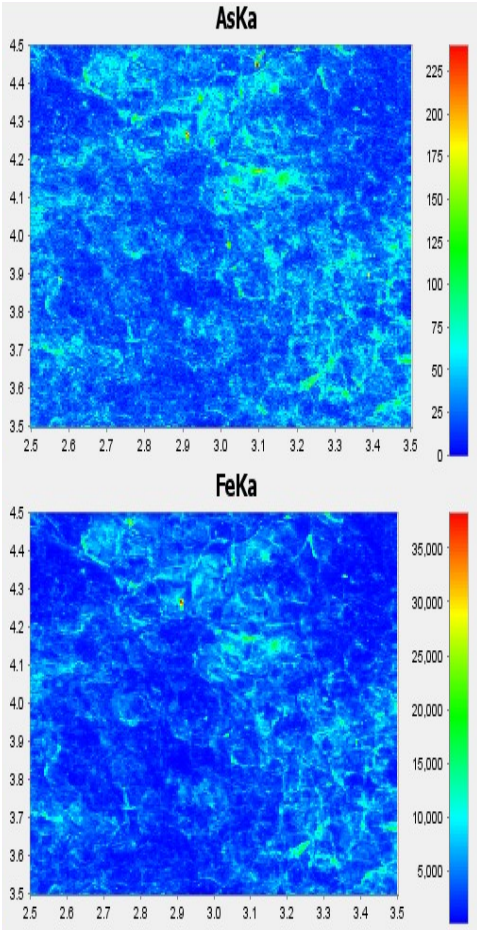

Figure S8. Representative μ-XRF elemental distribution maps showing correspondence of Fe-As hotspots. These display As scavenging by Fe(III) phases synthesized in chronoamperometric assays after 48 h, and retained on filtrates.

References

1 R. M. Atlas, Handbook of Microbiological Media, *Handbook of Microbiological Media*, , DOI:10.1201/EBK1439804063.

2 A. L. Leber, in *Clinical Microbiology Procedures Handbook*, John Wiley & Sons, Ltd, 2016.

3 A. Apler, I. Snowball, P. Frogner-Kockum and S. Josefsson, Distribution and dispersal of metals in contaminated fibrous sediments of industrial origin, *Chemosphere*, 2019, **215**, 470–481.

4 W. de Nolf, F. Vanmeert and K. Janssens, XRDUA: crystalline phase distribution maps by two-dimensional scanning and tomographic (micro) X-ray powder diffraction, *urn:issn:1600-5767*, 2014, **47**, 1107–1117.

5 B. Lafuente, R. T. Downs, H. Yang and N. Stone, in *Highlights in mineralogical crystallography*, eds. T. Armbruster and R. M. Danisi, De Gruyter, Berlin, 2016, pp. 1–30.

6 B. Ravel and M. Newville, ATHENA, ARTEMIS, HEPHAESTUS: data analysis for X-ray absorption spectroscopy using IFEFFIT, *urn:issn:0909-0495*, 2005, **12**, 537–541.